Author Manuscript

Author Manuscript

Author Manuscript

Author Manuscript

HHS Public Access

Author manuscript

PET Clin. Author manuscript; available in PMC 2020 January 07.

Published in final edited form as:

PET Clin. 2018 October ; 13(4): 551–565. doi:10.1016/j.cpet.2018.05.008.

MR Imaging of the Musculoskeletal System Using Ultrahigh Field (7T) MR Imaging

Hamza Alizai, MD[*], **Gregory Chang, MD**, **Ravinder R. Regatte, PhD**

Department of Radiology, New York University Langone Medical Center, 660 First Avenue, New York, NY 10016, USA

Keywords

MR imaging; 7T; Bone; Muscle; Cartilage

INTRODUCTION

In vivo musculoskeletal MR imaging plays a critical role in the modern medical practice. The excellent soft tissue contrast and multiplanar and multiparametric capabilities of MR imaging contribute to an unparalleled evaluation of all musculoskeletal tissues. Since the advent of diagnostic MR imaging, one of the most significant technological advancements has been the progressive increase in field strength (B_0) of the clinical MR imaging systems. MR imaging at higher field strength offers several advantages, including increased signal-to-noise ratio (SNR), higher spatial resolution, improved spectral resolution, improved sensitivity for X-nucleus imaging, and decreased image acquisition times.[1] The physics of imaging at higher field strengths also, however, poses technical challenges, some of which include radiofrequency (RF) coil design, increased chemical shift and susceptibility artifacts, increased RF energy deposition (specific absorption rate [SAR]), and changes in relaxation times compared with the lower field strength scanners.

In October 2017, the US Food and Drug Administration (FDA) approved the first 7T-Magnetom Terra (Siemens, Munich, Germany) MR imaging system for clinical diagnostic imaging of the head and the extremities. In this timely narrative review, we discuss the many potential opportunities as well as the challenges presented by 7T MR imaging systems. We also highlight recent developments in in vivo imaging of musculoskeletal tissues, including anatomic, structural, compositional, and functional imaging of cartilage, bone, and skeletal muscle, using these systems.

TECHNICAL ADVANTAGES AT HIGHER FIELD STRENGTHS

The SNR is often referred to as the “currency” of MR imaging and is an objective measure of image quality. Increasing SNR has been the primary driving force behind the development

[*]Corresponding author. Hamza.Alizai@nyumc.org.

Conflict of Interest Statement: The authors certify that they have no affiliations with or involvement in any organization or entity with any financial interest or nonfinancial interest in the subject matter or materials discussed in this article.

Author Manuscript Author Manuscript Author Manuscript Author Manuscript

of higher field strength MR systems. Increasing field strength results in increased magnetization (also referred to as spin polarization), which provides a higher SNR and improved resolution.[2] Magnetization can be expressed by the following formula:

$$M_0 = B_0\left(\gamma^2\hbar^2/4\kappa T\right)P_D$$

where P_D is proton spin density, γ represents the gyromagnetic ratio, $\hbar$ is Plank constant divided by 2π, k is the Boltzmann constant, T is the absolute temperature (Kelvin), and B_0 is the static magnetic field strength. The importance of field strength for magnetization can be easily delineated from the described formula. The calculation of SNR increase with increasing field strengths is, however, quite complicated and a detailed discussion can be found in the chapter by Collins[1] titled “Radio-frequency field calculations for high-field MR imaging.” For those of us who prefer a simple statistic, moving from 3T to 7T results in a gain of SNR by a factor of approximately 2.3.[3] This SNR gain translates to greater spatial resolution as well as reduced scan times, because SNR scales with square root of acquisition time.[3] Additionally, higher field strength allows parallel imaging to be performed with higher speed reduction factors, which can further reduce acquisition time.[4]

The SNR gain at 7T also improves the spectral resolution of (^{1}H) magnetic resonance spectroscopy (MRS), allowing identification of biological molecules that would not be possible at lower field strengths.[5] Furthermore, there are many biologically relevant nuclei besides ^{1}H, such as sodium and phosphorous, which occur in lower concentrations and are therefore difficult to image at conventional clinical field strengths. The utility of 7T in evaluating these nuclei has already been shown. Sodium is closely associated with the glycosaminoglycan, an important component of the cartilage extracellular matrix. Sodium (^{23}Na) MR imaging of cartilage at 7T has been used to map the sodium distribution and therefore indirectly detects early cartilage damage.[6] Phosphorous (^{31}P) is an important skeletal muscle metabolite and localized dynamic (^{31}P) MRS at 7T has been used to study mitochondrial oxidative metabolism in vivo.[7]

TECHNICAL CHALLENGES AT HIGHER FIELD STRENGTHS

Besides the enormous cost of acquiring and operating a 7T MR imaging system, there are technical challenges that need to be overcome for it to be routinely used in clinical imaging. Five of these are described. First, inhomogeneous tissue excitation is a problem at 7T and RF-related artifacts have been described in multiple in vivo studies.[8] At 7T, RF frequencies are higher, and wavelengths may be shorter than the object of interest, resulting in decreased penetration and inhomogeneous excitation. Artifacts may result with the B_1 magnitude and signal intensity much higher in the center of the field than at the periphery, therefore distorting the image.[8] These effects are more likely to be seen in the head or body than the extremities, which on average have smaller dimensions. RF coils for 7T MR imaging must be designed to control RF field propagation and minimize energy deposition.[9] RF shimming and parallel RF transmission techniques may be used to improve image quality at 7T.[10,11]

Author Manuscript Author Manuscript Author Manuscript Author Manuscript

Second, increasing field strength leads to changes in relaxation times; T_1 values increase[12] while T_2 values decrease.[13] Pulse sequences, therefore, need to be optimized to produce images with the contrast necessary to answer the diagnostic inquiry. Third, there is an increased sensitivity to susceptibility effects (decreased T_2*) at higher field strengths.[13] Although this may be beneficial for susceptibility-weighted imaging, susceptibility artifact related to orthopedic hardware can hinder interpretation of clinical MR imaging. Both conventional static B_0 and dynamic shimming[14] can be used to reduce susceptibility effects.

Fourth, there is a substantial increase in chemical shift artifact in the frequency-encoded direction at 7T.[15] The chemical shift difference between water and fat resonance is 1040 Hz at 7T compared with 440 Hz at 3T, which at a bandwidth of 130 Hz/pixel amounts to a chemical shift of 8 pixels at 7T versus 3.4 pixels at 3T.[15] The increase in chemical shift improves spectral resolution of MRS; however, chemical shift artifact may hinder interpretation of clinical images. Several techniques, such as using adiabatic refocusing pulses[16] have been used to reduce chemical shift displacement artifacts, but resulting in increases in SAR.

Last, but most importantly, patient safety is paramount. Increased RF at 7T results in higher energy (heat) deposition in tissues. SAR is the measure of RF absorption and scales with essentially the square of the magnetic field. At 7T, SAR needs close monitoring to avoid tissue heating. The FDA has established limits for SAR for both pediatric and adult patients.[17] Although the FDA considers MR imaging under 8T to pose no health risk to adults and children older than 1 month, minor side effects have been reported at high field strengths.[18,19] Table 1 provides a brief summary of some of the advantages and disadvantages of imaging at higher field strengths.

CARTILAGE

Cartilage Microarchitecture

Cartilage is composed of 70% to 80% fluid. The remainder is the extracellular matrix (ECM), a network of collagen fibrils and proteoglycan molecules. Proteoglycans consist of negatively charged glycosaminoglycan (GAGs) attached to protein core.[20] Cations such as sodium (Na^+) counter the negative charge of GAGs and maintain neutrality. The flow of water within the ECM provides the known biomechanical properties of cartilage.[21] In osteoarthritis (OA), the initial histologic changes include cartilage breakdown with proteoglycan loss and disorganization and/or loss of the collagen fiber network.[22]

Morphologic Imaging of Cartilage

Standard protocols for imaging cartilage morphology at 7T are yet to be established; however, will foreseeably follow the techniques used with 3T MR imaging systems. Springer and colleagues[23] recently performed comparable routine knee imaging at 3T and 7T and found diagnostic confidence of radiologists for cartilage defects to be higher with 7T. The turbo spin echo (TSE) pulse sequence used in this study is the workhorse for the clinical musculoskeletal imaging due to its excellent soft tissue contrast and rapid acquisition. Fast Spin Echo and TSE are also part of the International Cartilage Repair Society's cartilage

Author Manuscript Author Manuscript Author Manuscript Author Manuscript

imaging protocol.[24] Fat saturation is also essential for clinical musculoskeletal imaging and chemical shift selective fat saturation is easier to perform at 7T.

An in-plane resolution of 0.3 mm resolves the earliest fraying of the cartilage surface.[25] Jin and colleagues[26] acquired high-resolution 2-dimensional (2D) and 3D image of the knee and ankle joints at 7T with a 0.3 mm in-plane resolution for TSE and 0.47 mm for isotropic sequences, such as dual echo steady state (3D-DESS). The open architecture 8-channel transmit-receive coil in this study even allowed dynamic imaging during continuous knee and ankle flexion-extension cycles. Regatte and Schweitzer[15] previously described the acquisition of sagittal knee images with a resolution of 0.25 mm using a gradient-based isotropic fast low-angle shot pulse sequence (3D-FLASH) with fat suppression.

Isotropic sequences obviate the need for multiplanar acquisition and reduce acquisition time.[27] The diagnostic accuracy of isotropic fast spin echo (FSE) for cartilage morphology is similar to 2D FSE at 3T; however, this remains to be studied for images obtained at 7T.[28] Other isotropic sequences, including 3D spoiled gradient recoiled echo (SPGR) and 3D-FLASH produce images with cartilage signal more intense than the surrounding tissues[26] and may be better suited for quantitative analysis of cartilage rather than morphologic assessment (Fig. 1).[29–31]

Compositional Imaging of Cartilage

By the time morphologic changes in cartilage are evident on clinical MR imaging, cartilage degeneration is in its advanced stages. Compositional imaging techniques have primarily been used in few research centers; however, allow detection of biochemical and microstructural changes in the cartilage ECM. These methods can, therefore, help identify cartilage breakdown at its earliest stages. We briefly describe some of these techniques and related recent developments at 7T.

T_2 Mapping and T_2* Mapping

T_2 mapping has been the most widely studied of all compositional imaging techniques and was an integral part of the knee imaging protocol in the large multicenter osteoarthritis initiative cohort study.[32] After application of an RF pulse, the rate constant of dephasing in the transverse plane equates to T_2 relaxation time. This value measured in milliseconds reflects water content and indirectly the collagen content in the cartilage ECM.[33] There is a laminar variation of T_2 values in cartilage with higher values at the articular surface compared with the bone interface.[34] Higher cartilage T_2 values have been shown to be predictive of the development of morphologic changes of cartilage deterioration.[35]

Welsch and colleagues[36] found less variation in T_2 measurements performed at 7T. This study reported cartilage T_2 values to be intrinsically lower compared with 3T and the laminar variation to be less pronounced. T_2 mapping at 7T has been shown to be able to discriminate between repaired knee cartilage and adjacent healthy cartilage (Fig. 2).[37–39] It has also been shown to detect maturation of reparative tissue after autologous chondrocyte transplantation.[40] Additionally, the increased resolution and decreased partial volume effects at 7T may allow T_2 and T_2* mapping of thinner cartilage in the hips and ankles.[41] Juras and colleagues[42] have compared within-subject T2 values in the knee and ankle cartilage at 7T

Author Manuscript Author Manuscript Author Manuscript Author Manuscript

and found these to be significantly different owing to their varying biomechanical and biochemical properties.

T_2* mapping measures transverse-plane dephasing using multi-echo gradient echo techniques, which are faster to acquire than T_2 but are also more vulnerable to local field inhomogeneity.[36,43] T_2* values are also lower at 7T than at 3T.[36] Both T_2 and T_2* are affected by magic angle effect; that is, the values increase as the angle between collagen fibers and B_0 approaches 55°.

T1rho Mapping

T1rho evaluates the spin-lattice (T_1) relaxation in the rotating frame.[44] It can evaluate the interaction between free (bulk) water and adjacent molecules and is understood to reflect particularly the proteoglycan content of the ECM.[45] T1rho, like T_2, predicts morphologic deterioration of articular cartilage.[46] T1rho imaging is more challenging to perform due to B_0 and B_1 inhomogeneity, specialized RF pulse sequence requirements, and long acquisition times. The long scan time is particularly a concern at 7T due to increased SAR. A recent study, however, leveraged the SNR advantage of 7T to acquire high-resolution T1rho images (0.2 mm^2 in-plane resolution) in reasonable acquisition times (<30 minutes) and within SAR constraints.[47] This study reported T1rho times lower at 7T than at 3T. It also found T1rho values to be higher in the medial femoral condyles of volunteers with meniscal tears compared with those without tears. Wyatt and colleagues[48] found T1rho values to be higher in patients with OA compared with healthy subjects, with the differences being higher and statistically significant in more regions at 7T than at 3T. Kogan and colleagues[49] compared T1-rho at 7T to the gagCEST sequence (described later in this article) and reported good agreement between the 2 techniques. The same investigators have also described combining the 2 methods at 7T to form a CESTrho sequence, which can quantify proton exchange at intermediate exchange rates, without being affected by confounding factors, which can affect proton exchange rates.[50]

Ultrashort Echo Time and Zero Echo Time Imaging

Musculoskeletal tissues such as cortical bone, tendon, ligaments, and the deep calcified part of cartilage contain a high fraction of components with “ultrashort” transverse relaxation times and therefore produce no signal on standard MR images as their signal decays before it can be acquired.[51] Ultrashort echo time (UTE) and zero echo time use specialized acquisition and reconstruction techniques to capture these ultrashort components before signal decay. The application of these techniques at 7T has primarily focused on tendons and cortical bone. At lower field strengths, UTE has been used to delineate the calcified deepest cartilage layer[52] and has also been used to evaluate the integrity of this layer in osteochondral allografts.[53] UTE also enables T_2 and T_2* mapping of tissues with a high fraction of ultrashort components. Chu and colleagues[54] reported UTE T_2* to be helpful in evaluating cartilage healing after anterior cruciate ligament reconstruction.

Delayed Gadolinium-Enhanced MR Imaging of Cartilage

Gadopentetate dimeglumine (Gd-$DTPA^{2-}$), the commonly used MR imaging contrast, is an anion and therefore repelled by the negatively charged GAGs. dGEMRIC takes advantage of

Author Manuscript Author Manuscript Author Manuscript Author Manuscript

this to map GAG content within cartilage. An area of damaged cartilage will accumulate Gd-DTPA^{2-} and therefore have a shorter T_1 relaxation time. In vivo delayed gadolinium-enhanced MR imaging of cartilage (dGEMRIC) studies at 7T are scarce. A feasibility study by Welsch and colleagues[39] found dGEMRIC to be promising at 7T. In this study of 5 healthy volunteers, T1 values differed between tibial and femoral cartilage.

At lower field strengths, dGEMRIC has been used for a wide range of musculoskeletal conditions, including cartilage repair,[55,56] tibial osteotomy,[57] inflammatory arthritis,[58] and chronic joint unloading.[59]

The disadvantages of dGEMRIC include the large doses of Gd-DTPA^{2-} required. There is also the delay between injection, joint exercise for efficient diffusion into the joint, and long acquisition times.[60] There is, however, a possibility of obtaining an indirect MR arthrogram during this delay, which can aid morphologic evaluation of intra-articular structures, particularly the hip labrum. A recent study by Lazik-Palm and colleagues[61] found that gadolinium administration at 7T did not significantly impact either T_2 or T_2* relaxation times and improved morphologic image quality. The investigators suggest morphologic and quantitative analysis including dGEMRIC can, therefore, be combined to perform a comprehensive examination during a single visit.

Sodium (^{23}Na) Imaging

The negatively charged GAGs in cartilage ECM attract positive $^{23}Na^{+}$ counter-ions, the distribution of which reflect local GAG concentration. Loss of GAG content with cartilage degeneration will result in a lower concentration of $^{23}Na^{+}$ ions.[62] ^{23}Na has a spin magnetic moment; however, its concentration is only 0.08% that of ^{1}H, which makes it difficult to elicit signal, resulting in noisy MR images and long acquisition times. The SNR gain at 7T MR imaging is hence particularly useful for ^{23}Na imaging, as it increases its sensitivity[63] and improves resolution. ^{23}Na imaging has been shown to correlate well with dGEMRIC.[64] Unlike dGEMRIC, ^{23}Na imaging can assess cartilage proteoglycan without intravenous contrast injection. The Larmor frequency of $^{23}Na^{+}$ is much lower than that of ^{1}H, so specialized transmit-receive coils are, however, required.[65] SAR is also a concern with sodium imaging at long acquisition times; however, Medelin and colleagues[66] have demonstrated that compressed sensing image reconstruction can reduce scan times to less than 10 minutes without losing sodium quantification accuracy. Additionally, sodium inversion recovery pulse sequences can be designed to mitigate RF absorption while improving quality through suppression of free sodium in the synovial fluid.[67,68] As with T_2 Mapping, sodium imaging has been shown to be able to discriminate between cartilage repair tissue and healthy cartilage (Fig. 3).[68,69] The investigators of this study reported lower sodium signal intensity in repair tissue after microfracture surgery or matrix autologous chondrocyte transplantation (MACT) compared with healthy cartilage, suggesting diminished GAG content. A different study by the same group found repair tissue after MACT to have higher sodium signal intensity than after bone marrow stimulation, leading them to imply that MACT repair is of better quality.[70]

Author Manuscript Author Manuscript Author Manuscript Author Manuscript

Diffusion Tensor Imaging

The cartilage collagen network is highly organized resulting in anisotropic water diffusion within the ECM. Diffusion tensor imaging (DTI) can assess both proteoglycan content through mean apparent diffusion coefficient (ADC) and collagen microarchitecture through fractional anisotropy (FA). Raya and colleagues[71] used a line-scan DTI imaging sequence at 7T to compare articular cartilage of healthy subjects with cartilage in subjects with osteoarthritis. They found that both mean ADC and FA values to be good discriminators between the groups, with FA having higher specificity. Ex vivo imaging performed by the same group at 17.6 T found DTI to be excellent for detecting cartilage damage (95% accuracy) and demonstrate good performance for grading cartilage damage (75% accuracy). [72] DTI imaging of cartilage is overall challenging to perform in vivo owing to the short T2 of articular cartilage and the high resolution needed to depict the cartilage anatomy.

Glycosaminoglycan Chemical Exchange Saturation Transfer Imaging

Water protons bound to macromolecules exchange their magnetization with free water protons within the ECM. Water protons bound to macromolecules have unique RF frequency and can be saturated using off-resonance RF pulses. Subsequently, the magnetization exchange with free water results in a loss of image signal intensity, and this effect can be measured to estimate local macromolecule content. With GAG chemical exchange saturation transfer imaging (gagCEST), GAGs are the macromolecules being evaluated with the off-resonance RF saturation pulses applied to saturate exchangeable protons residing on the hydroxyl groups of cartilage GAGs (Fig. 4).[73] gagCEST has been shown to be sensitive to cartilage proteoglycan content.[73] It also correlates well with $^{23}Na^{+}$ imaging and feasible at 7T.[74] Singh and colleagues[75] compared CEST in knee cartilage at 3T and 7T and found CEST measurements to be negligible at 3T, whereas the results were more promising at 7T. Kogan and colleagues[49] recently described a volumetric multislice gagCEST technique, which can reduce acquisition time.

SKELETAL MUSCLE

Morphologic Images of Skeletal Muscle

Morphologic imaging of skeletal muscle at 7T is similar to imaging at lower field strengths. Routine clinical protocols will need to be optimized to maintain contrast desired by the radiologists to respond to the diagnostic inquiries.

Chemical-Shift-Encoded Water-Fat Separation MR Imaging

As previously described, chemical shift is increased at 7T resulting in improved spectral resolution. Chemical-shift-encoded water-fat separation (WFI) techniques have been used for intramuscular adipose tissue quantification. WFI captures the phase difference between water and fat protons by acquiring ≥2 echoes and can provide high-resolution 3D imaging of fat composition.[76] This technique is yet to be applied in vivo in human subjects at 7T. At lower field strengths, fat-fraction (FF) estimated using WFI is reliable in comparison with biopsy[77] and more accurate than visual fat grading.[78] The distribution of MR imaging measured intramuscular fat is different in type 2 diabetes compared with healthy subjects[79]

Author Manuscript Author Manuscript Author Manuscript Author Manuscript

and intramuscular FF also progressively increases in patients with neuromuscular disorders. Quadriceps muscle FF is associated with osteoarthritis,[80] whereas shoulder rotator cuff muscle FF correlates with the success of repair as well with pain and range of motion.[81]

MR Spectroscopy

Glycogen, intramyocellular lipid (IMCL), and extramyocellular lipid (EMCL) and phosphocreatine (PCr) are all sources of energy for skeletal muscle, which can be measured in vivo using ^{13}C, ^{1}H, and ^{31}P MR spectroscopy (MRS).[82] The frequency difference between IMCL and EMCL is too small to delineate with chemical-shift imaging but can be assessed with ^{1}H MRS.[83] At 7T, the increased resolution of lipid spectra allows identification of additional lipid peaks, which are not visible at lower field strengths.[84] Compared with 3T, the T_1 relaxation times of skeletal muscle metabolites are increased at 7T, whereas T_2 relaxation times are decreased.[84] MRS is particularly of interest to endocrinologists, as IMCL levels are elevated in subjects with insulin resistance.[83]

^{31}P MRS provides information about skeletal muscle bioenergetics. It can detect phosphorylated compounds including phosphocreatine (PCr), inorganic phosphates (Pi), the phosphate groups in ATP, and phosphomonoesters (Fig. 5). The advantages of performing this technique at 7T are clear. Bogner and colleagues[85] found 7T ^{31}P MRS in the human calf muscle has shorter measurement times with increased SNR and improved temporal resolution in dynamic studies. Parasoglou and colleagues[86] developed a spectrally selective 3D TSE sequence, which can provide simultaneous measurement of PCr resynthesis rates in several muscles of the exercising body part. ^{31}P MRS has shown that athletes have higher PCr/Pi ratios for a given workload and a faster recovery of PCr.[87] Both of these measurements have been proposed to provide MR-based functional measures of mitochondrial density.[88] ^{31}P MRS has also been used as a tool to study several diseases, including peripheral arterial disease[89] and type 2 diabetes.[90]

T_2 Mapping

The advantages of skeletal muscle T_2 mapping at 7T remain to be determined. Preliminary work, including optimization of sequence parameters and the determination of how perfusion and oxygenation might affect T_2 mapping at 7T, is ongoing.[91] Theoretically, the higher spatial resolution would allow more accurate and more automated for quantitative analysis. A preliminary study at New York University performed T2 mapping in a small cohort of volunteers after plantar flexion exercises and found T2 values to decrease after exercise. The calculated T2 values for skeletal muscle and the time course of recovery for T2 values after exercise were similar to those described at lower field strength.[9]

At lower field strengths, T2 mapping has been shown to correlate with nonquantitative MR scores for fatty infiltration and proposed as a potential imaging biomarker for neuromuscular disorders, such as Duchene muscular dystrophy[92] and Pompe disease.[93] It also may be valuable for measuring therapeutic effects of corticosteroids on the skeletal muscle in these patients.[94]

Author Manuscript Author Manuscript Author Manuscript Author Manuscript

^{23}Na MR Imaging

Sodium concentration gradients across the cell membrane contribute to the resting membrane potential and help generate action potentials leading to muscle contraction.[9] The general challenges of sodium imaging, as well as advantages of 7T sodium MR imaging, were previously discussed in the cartilage section. The feasibility of 23Na MR imaging at 7T was demonstrated by Chang and colleagues[95] in a study comparing the effect of exercise on skeletal muscle sodium concentrations in healthy subjects and diabetic individuals. Sodium signal intensity increased within the muscle in both groups after exercise; however, the diabetic individuals demonstrated a delayed return to preexercise sodium signal intensity.

At lower field strengths, ^{23}Na MR imaging has been used to study skeletal muscle in health volunteers as well as patients with neuromuscular disorders such as Duchenne muscular dystrophy[96] and paramyotonia congentia.[97] Increased sodium signal intensity in the skeletal muscle of patients with the neuromuscular disorder has been proposed as being a contributor to the pathogenesis via intracellular muscle edema.

BONE

Osteoporosis is characterized by a decrease in bone mineral density (BMD) resulting in susceptibility to fragility fractures.[98] Dual-energy x-ray absorptiometry (DXA), the current screening standard for osteoporosis, may artificially underestimate or overestimate fracture risk.[99] A big component of bone imaging research, therefore, focuses on establishing better measures of bone quality and strength and improving prediction of fragility fractures. Normal bone is composed of an outer compact cortical component, internal trabecular component, and bone marrow. The SNR gain and increased resolution of 7T makes it easier to quantify apparent trabecular structural parameters. MR imaging of trabecular bone has been validated via comparisons with micro-computed tomography and histology,[100,101] and these measurements have also been shown to be reproducible.[102] Chang and colleagues[103] demonstrated the feasibility of performing a comprehensive hip MR imaging protocol at 7T that included high-resolution imaging of bone microarchitecture and cartilage, as well as clinical imaging. They also found that same 7T MR imaging of bone microarchitecture can discriminate between women without and with fragility fractures who do not differ by DXA-derived BMD (Fig. 6).[104,105] On the other hand, a study of bone microarchitecture in Olympic fencing athletes found them to have better bone quality than controls.[106] Micro–finite element analysis (FEA), traditionally an engineering tool, has also been performed on 7T high-resolution MR imaging of the distal tibia and proximal femur. MR imaging–based FEA provides bone stiffness measures as a potential imaging marker for bone strength.[107] Professional dancers, for example, were found to have increased bone stiffness in comparison with inactive controls.[108] Feasibility of performing these bone MR imaging techniques at 7T in smaller joints such as the wrist has been demonstrated.[109]

Due to its short T_2 components, cortical bone demonstrates low signal on routine MR imaging. UTE can, however, improve assessment of cortical bone and at lower field strengths has been successfully applied to study cortical water content, which is related to cortical porosity.[110,111] A feasibility study by Krug and colleagues[3] used an isotropic UTE sequence at 7T and 3T. The investigators reported an SNR gain by a factor of 1.7 (from 3T

Author Manuscript Author Manuscript Author Manuscript Author Manuscript

to 7T) and significantly shorter T_2 values. Further studies are needed to fully explore the potential of UHF MR imaging for imaging cortical bone.

SUMMARY

The recent approval of 7T MR imaging for clinical use is a major advancement that will drive the development of both clinical and research applications for musculoskeletal imaging. The SNR gain at 7T is an irrefutable advantage. The technical challenges are plentiful but RF inhomogeneity and coil design are the 2 that are underlined. Future musculoskeletal imaging protocols will likely include a combination of clinical morphologic and compositional imaging sequences. Advancement of compositional imaging techniques at 7T will likely be rapid. Further development of CEST techniques will enable high-resolution imaging of organic molecules, such as glucose and proteins, which play critical roles in disease pathogenesis. Higher SNR will permit X-nuclei MRS, including ^{23}Na, ^{39}K, ^{31}P, ^{13}C, ^{17}O, and so on, which will provide vital information regarding cellular processes, metabolic turnovers, energy metabolism, and oxygen consumption rate. MR imaging at 7T is another big step in the continued drive toward precision personalized medicine.

REFERENCES

1. Collins C Radiofrequency field calculations for high field MRI In: Robitaille PM, Berliner LJ, editors. Ultra High Field Magnetic Resonance Imaging. New York: Springer; 2006 p. 209–48.
2. Moser E, Stahlberg F, Ladd ME, et al. 7-T MR—from research to clinical applications? NMR Biomed 2012;25(5):695–716. [PubMed: 22102481]
3. Krug R, Stehling C, Kelley DA, et al. Imaging of the musculoskeletal system in vivo using ultra-high field magnetic resonance at 7 T. Invest Radiol 2009;44(9):613–8. [PubMed: 19652609]
4. Wiesinger F, Van de Moortele P-F, Adriany G, et al. Potential and feasibility of parallel MRI at high field. NMR Biomed 2006;19(3):368–78. [PubMed: 16705638]
5. Scheenen TW, Heerschap A, Klomp DW. Towards 1H-MRSI of the human brain at 7T with slice-selective adiabatic refocusing pulses. MAGMA 2008;21(1–2):95–101. [PubMed: 18210177]
6. Staroswiecki E, Bangerter NK, Gurney PT, et al. In vivo sodium imaging of human patellar cartilage with a 3D cones sequence at 3 T and 7 T. J Magn Reson Imaging 2010;32(2):446–51. [PubMed: 20677276]
7. Meyerspeer M, Robinson S, Nabuurs CI, et al. Comparing localized and nonlocalized dynamic 31P magnetic resonance spectroscopy in exercising muscle at 7 T. Magn Reson Med 2012;68(6):1713–23. [PubMed: 22334374]
8. Van de Moortele P-F, Akgun C, Adriany G, et al. B1 destructive interferences and spatial phase patterns at 7 T with a head transceiver array coil. Magn Reson Med 2005;54(6):1503–18. [PubMed: 16270333]
9. Chang G, Wang L, Cardenas-Blanco A, et al. Biochemical and physiological MR imaging of skeletal muscle at 7 tesla and above. Semin Musculoskelet Radiol 2010;14(2):269–78. [PubMed: 20486034]
10. Setsompop K, Alagappan V, Zelinski AC, et al. High-flip-angle slice-selective parallel RF transmission with 8 channels at 7 T. J Magn Reson 2008;195(1): 76–84. [PubMed: 18799336]
11. Hsu YC, Chu YH, Chern IL, et al. Mitigate B(1)(+) inhomogeneity by nonlinear gradients and RF shimming. Conf Proc IEEE Eng Med Biol Soc 2013;2013:1085–8. [PubMed: 24109880]
12. Jordan CD, Saranathan M, Bangerter NK, et al. Musculoskeletal MRI at 3.0 T and 7.0 T: a comparison of relaxation times and image contrast. Eur J Radiol 2013;82(5):734–9. [PubMed: 22172536]
13. Pruessmann KP. Parallel imaging at high field strength: synergies and joint potential. Top Magn Reson Imaging 2004;15(4):237–44. [PubMed: 15548954]

Author Manuscript Author Manuscript Author Manuscript Author Manuscript

14. Sengupta S, Welch EB, Zhao Y, et al. Dynamic B0 shimming at 7 T. Magn Reson Imaging 2011;29(4): 483–96. [PubMed: 21398062]
15. Regatte RR, Schweitzer ME. Ultra-high-field MRI of the musculoskeletal system at 7.0T. J Magn Reson Imaging 2007;25(2):262–9. [PubMed: 17260399]
16. Balchandani P, Spielman D. Fat suppression for 1H MRSI at 7Tusing spectrally selective adiabatic inversion recovery. Magn Reson Med 2008;59(5):980–8. [PubMed: 18429027]
17. U.S. Department of Health and Human Services, Food and Drug Administration, Center for Devices and Radiological Health, Guidance for Industry and FDA Staff. Criteria for significant risk investigations of magnetic resonance diagnostic devices, 6 20, 2014.
18. Chakeres DW, Kangarlu A, Boudoulas H, et al. Effect of static magnetic field exposure of up to 8 Tesla on sequential human vital sign measurements. J Magn Reson Imaging 2003;18(3):346–52. [PubMed: 12938131]
19. de Vocht F, Stevens T, Glover P, et al. Cognitive effects of head-movements in stray fields generated by a 7 Tesla whole-body MRI magnet. Bio-electromagnetics 2007;28(4):247–55.
20. Binks DA, Hodgson RJ, Ries ME, et al. Quantitative parametric MRI of articular cartilage: a review of progress and open challenges. Br J Radiol 2013; 86(1023):20120163. [PubMed: 23407427]
21. Sophia Fox AJ, Bedi A, Rodeo SA. The basic science of articular cartilage: structure, composition, and function. Sports Health 2009;1(6):461–8. [PubMed: 23015907]
22. Buckwalter JA, Mankin HJ. Articular cartilage: degeneration and osteoarthritis, repair, regeneration, and transplantation. Instr Course Lect 1998; 47:487–504. [PubMed: 9571450]
23. Springer E, Bohndorf K, Juras V, et al. Comparison of routine knee magnetic resonance imaging at 3 T and 7 T. Invest Radiol 2017;52(1):42–54. [PubMed: 27434621]
24. Bobic V ICRS articular cartilage imaging committee. ICRS MR imaging protocol for knee articular cartilage. 2000;12.
25. Rubenstein JD, Li JG, Majumdar S, et al. Image resolution and signal-to-noise ratio requirements for MR imaging of degenerative cartilage. AJR Am J Roentgenol 1997;169(4):1089–96. [PubMed: 9308470]
26. Jin J, Weber E, Destruel A, et al. An open 8-channel parallel transmission coil for static and dynamic 7T MRI of the knee and ankle joints at multiple postures. Magn Reson Med 2018;79(3): 1804–16. [PubMed: 28643359]
27. Mugler JP 3rd. Optimized three-dimensional fast-spin-echo MRI. J Magn Reson Imaging 2014; 39(4):745–67. [PubMed: 24399498]
28. Kijowski R, Davis KW, Woods MA, et al. Knee joint: comprehensive assessment with 3D isotropic resolution fast spin-echo MR imaging–diagnostic performance compared with that of conventional MR imaging at 3.0 T. Radiology 2009;252(2):486–95. [PubMed: 19703886]
29. Mohr A The value of water-excitation 3D FLASH and fat-saturated PDw TSE MR imaging for detecting and grading articular cartilage lesions of the knee. Skeletal Radiol 2003;32(7):396–402. [PubMed: 12719928]
30. Blankenbaker DG, Ullrick SR, Kijowski R, et al. MR arthrography of the hip: comparison of IDEAL-SPGR volume sequence to standard MR sequences in the detection and grading of cartilage lesions. Radiology 2011;261(3):863–71. [PubMed: 21900621]
31. Regatte RR, Schweitzer ME. Novel contrast mechanisms at 3 tesla and 7 tesla. Semin Musculoskelet Radiol 2008;12(3):266–80. [PubMed: 18850506]
32. Peterfy CG, Schneider E, Nevitt M. The osteoarthritis initiative: report on the design rationale for the magnetic resonance imaging protocol for the knee. Osteoarthritis Cartilage 2008;16(12):1433–41. [PubMed: 18786841]
33. Liess C, Lusse S, Karger N, et al. Detection of changes in cartilage water content using MRI T2-mapping in vivo. Osteoarthritis Cartilage 2002; 10(12):907–13. [PubMed: 12464550]
34. Carballido-Gamio J, Blumenkrantz G, Lynch JA, et al. Longitudinal analysis of MRI T(2) knee cartilage laminar organization in a subset of patients from the osteoarthritis initiative. Magn Reson Med 2010;63(2):465–72. [PubMed: 19918905]
35. Joseph GB, Baum T, Alizai H, et al. Baseline mean and heterogeneity of MR cartilage T2 are associated with morphologic degeneration of cartilage, meniscus, and bone marrow over 3 years–

Author Manuscript Author Manuscript Author Manuscript Author Manuscript

data from the Osteoarthritis Initiative. Osteoarthritis Cartilage 2012;20(7):727–35. [PubMed: 22503812]

36. Welsch GH, Apprich S, Zbyn S, et al. Biochemical (T2, T2* and magnetisation transfer ratio) MRI of knee cartilage: feasibility at ultra-high field (7T) compared with high field (3T) strength. Eur Radiol 2011;21(6):1136–43. [PubMed: 21153551]
37. Chang G, Xia D, Sherman O, et al. High resolution morphologic imaging and T2 mapping of cartilage at 7 Tesla: comparison of cartilage repair patients and healthy controls. MAGMA 2013;26(6):539–48. [PubMed: 23657612]
38. Domayer SE, Apprich S, Stelzeneder D, et al. Cartilage repair of the ankle: first results of T2 mapping at 7.0 T after microfracture and matrix associated autologous cartilage transplantation. Osteoarthritis Cartilage 2012;20(8):829–36. [PubMed: 22542632]
39. Welsch GH, Mamisch TC, Hughes T, et al. In vivo biochemical 7.0 Tesla magnetic resonance: preliminary results of dGEMRIC, zonal T2, and T2* mapping of articular cartilage. Invest Radiol 2008;43(9): 619–26. [PubMed: 18708855]
40. Welsch GH, Mamisch TC, Marlovits S, et al. Quantitative T2 mapping during follow-up after matrix-associated autologous chondrocyte transplantation (MACT): full-thickness and zonal evaluation to visualize the maturation of cartilage repair tissue. J Orthop Res 2009;27(7):957–63. [PubMed: 19133648]
41. Lazik A, Theysohn JM, Geis C, et al. 7 Tesla quantitative hip MRI: T1, T2 and T2* mapping of hip cartilage in healthy volunteers. Eur Radiol 2016; 26(5):1245–53. [PubMed: 26314482]
42. Juras V, Zbyn S, Mlynarik V, et al. The compositional difference between ankle and knee cartilage demonstrated by T2 mapping at 7 Tesla MR. Eur J Radiol 2016;85(4):771–7. [PubMed: 26971422]
43. Mamisch TC, Hughes T, Mosher TJ, et al. T2 star relaxation times for assessment of articular cartilage at 3 T: a feasibility study. Skeletal Radiol 2012;41(3):287–92. [PubMed: 21499976]
44. Sepponen RE, Pohjonen JA, Sipponen JT, et al. A method for T1 rho imaging. J Comput Assist Tomogr 1985;9(6):1007–11. [PubMed: 4056129]
45. Keenan KE, Besier TF, Pauly JM, et al. Prediction of glycosaminoglycan content in human cartilage by age, T1rho and T2 MRI. Osteoarthritis Cartilage 2011;19(2):171–9. [PubMed: 21112409]
46. Prasad AP, Nardo L, Schooler J, et al. T(1)rho and T(2) relaxation times predict progression of knee osteoarthritis. Osteoarthritis Cartilage 2013;21(1): 69–76. [PubMed: 23059757]
47. Singh A, Haris M, Cai K, et al. High resolution T1rho mapping of in vivo human knee cartilage at 7T. PLoS One 2014;9(5):e97486. [PubMed: 24830386]
48. Wyatt C, Guha A, Venkatachari A, et al. Improved differentiation between knees with cartilage lesions and controls using 7T relaxation time mapping. J Orthop Translat 2015;3(4):197–204. [PubMed: 30035058]
49. Kogan F, Hargreaves BA, Gold GE. Volumetric multislice gagCEST imaging of articular cartilage: optimization and comparison with T1rho. Magn Reson Med 2017;77(3):1134–41. [PubMed: 26923108]
50. Kogan F, Singh A, Cai K, et al. Investigation of chemical exchange at intermediate exchange rates using a combination of chemical exchange saturation transfer (CEST) and spin-locking methods (CESTrho). Magn Reson Med 2012;68(1):107–19. [PubMed: 22009759]
51. Bae WC, Du J, Bydder GM, et al. Conventional and ultrashort time-to-echo magnetic resonance imaging of articular cartilage, meniscus, and intervertebral disk. Top Magn Reson Imaging 2010;21(5): 275–89. [PubMed: 22129641]
52. Bae WC, Dwek JR, Znamirowski R, et al. Ultrashort echo time MR imaging of osteochondral junction of the knee at 3 T: identification of anatomic structures contributing to signal intensity. Radiology 2010; 254(3):837–45. [PubMed: 20177096]
53. Chang EY, Pallante-Kichura AL, Bae WC, et al. Development of a Comprehensive Osteochondral Allograft MRI Scoring System (OCAMRISS) with histopathologic, micro-computed tomography, and biomechanical validation. Cartilage 2014;5(1):16–27. [PubMed: 24489999]

Author Manuscript Author Manuscript Author Manuscript Author Manuscript

54. Chu CR, Williams AA, West RV, et al. Quantitative magnetic resonance imaging UTE-T2* mapping of cartilage and meniscus healing after anatomic anterior cruciate ligament reconstruction. Am J Sports Med 2014;42(8):1847–56. [PubMed: 24812196]
55. Lazik A, Korsmeier K, Classen T, et al. 3 Tesla high-resolution and delayed gadolinium enhanced MR imaging of cartilage (dGEMRIC) after autologous chondrocyte transplantation in the hip. J Magn Reson Imaging 2015;42(3):624–33. [PubMed: 25522716]
56. Watanabe A, Wada Y, Obata T, et al. Delayed gadolinium-enhanced MR to determine glycosaminoglycan concentration in reparative cartilage after autologous chondrocyte implantation: preliminary results. Radiology 2006;239(1):201–8. [PubMed: 16484349]
57. d'Entremont AG, McCormack RG, Agbanlog K, et al. Cartilage health in high tibial osteotomy using dGEMRIC: relationships with joint kinematics. Knee 2015;22(3):156–62. [PubMed: 25715920]
58. Schleich C, Muller-Lutz A, Sewerin P, et al. Intra-individual assessment of inflammatory severity and cartilage composition of finger joints in rheumatoid arthritis. Skeletal Radiol 2015;44(4):513–8. [PubMed: 25367672]
59. Owman H, Tiderius CJ, Ericsson YB, et al. Long-term effect of removal of knee joint loading on cartilage quality evaluated by delayed gadolinium-enhanced magnetic resonance imaging of cartilage. Osteoarthritis Cartilage 2014;22(7):928–32. [PubMed: 24795270]
60. Burstein D, Velyvis J, Scott KT, et al. Protocol issues for delayed Gd(DTPA)(2-)-enhanced MRI (dGEMRIC) for clinical evaluation of articular cartilage. Magn Reson Med 2001;45(1):36–41. [PubMed: 11146483]
61. Lazik-Palm A, Kraff O, Geis C, et al. Morphological imaging and T2 and T2* mapping of hip cartilage at 7 Tesla MRI under the influence of intravenous gadolinium. Eur Radiol 2016;26(11): 3923–31. [PubMed: 26873493]
62. Madelin G, Lee JS, Regatte RR, et al. Methods and applications. Prog Nucl Magn Reson Spectrosc 2014;79:14–47. [PubMed: 24815363]
63. Madelin G, Babb J, Xia D, et al. Articular cartilage: evaluation with fluid-suppressed 7.0-T sodium MR imaging in subjects with and subjects without osteoarthritis. Radiology 2013;268(2):481–91. [PubMed: 23468572]
64. Trattnig S, Welsch GH, Juras V, et al. 23Na MR imaging at 7 T after knee matrix-associated autologous chondrocyte transplantation preliminary results. Radiology 2010;257(1):175–84. [PubMed: 20713608]
65. Wiggins GC, Brown R, Lakshmanan K. High-performance radiofrequency coils for (23)Na MRI: brain and musculoskeletal applications. NMR Biomed 2016;29(2):96–106. [PubMed: 26404631]
66. Madelin G, Chang G, Otazo R, et al. Compressed sensing sodium MRI of cartilage at 7T: preliminary study. J Magn Reson 2012;214(1):360–5. [PubMed: 22204825]
67. Lee JS, Xia D, Madelin G, et al. Sodium inversion recovery MRI on the knee joint at 7 T with an optimal control pulse. J Magn Reson 2016;262: 33–41. [PubMed: 26705907]
68. Chang G, Madelin G, Sherman OH, et al. Improved assessment of cartilage repair tissue using fluid-suppressed (2)(3)Na inversion recovery MRI at 7 Tesla: preliminary results. Eur Radiol 2012;22(6): 1341–9. [PubMed: 22350437]
69. Zbyn S, Brix MO, Juras V, et al. Sodium magnetic resonance imaging of ankle joint in cadaver specimens, volunteers, and patients after different cartilage repair techniques at 7 T: initial results. Invest Radiol 2015;50(4):246–54. [PubMed: 25436618]
70. Zbyn S, Stelzeneder D, Welsch GH, et al. Evaluation of native hyaline cartilage and repair tissue after two cartilage repair surgery techniques with 23Na MR imaging at 7 T: initial experience. Osteoarthritis Cartilage 2012;20(8):837–45. [PubMed: 22548796]
71. Raya JG, Horng A, Dietrich O, et al. Articular cartilage: in vivo diffusion-tensor imaging. Radiology 2012;262(2):550–9. [PubMed: 22106350]
72. Raya JG, Melkus G, Adam-Neumair S, et al. Diffusion-tensor imaging of human articular cartilage specimens with early signs of cartilage damage. Radiology 2013;266(3):831–41. [PubMed: 23238155]

Author Manuscript Author Manuscript Author Manuscript Author Manuscript

73. Ling W, Regatte RR, Navon G, et al. Assessment of glycosaminoglycan concentration in vivo by chemical exchange-dependent saturation transfer (gagCEST). Proc Natl Acad Sci U S A 2008; 105(7):2266–70. [PubMed: 18268341]
74. Schmitt B, Zbyn S, Stelzeneder D, et al. Cartilage quality assessment by using glycosaminoglycan chemical exchange saturation transfer and (23) Na MR imaging at 7 T. Radiology 2011;260(1): 257–64. [PubMed: 21460030]
75. Singh A, Haris M, Cai K, et al. Chemical exchange saturation transfer magnetic resonance imaging of human knee cartilage at 3 T and 7 T. Magn Reson Med 2012;68(2):588–94. [PubMed: 22213239]
76. Eggers H, Bornert P. Chemical shift encoding-based water-fat separation methods. J Magn Reson Imaging 2014;40(2):251–68. [PubMed: 24446249]
77. Gaeta M, Scribano E, Mileto A, et al. Muscle fat fraction in neuromuscular disorders: dual-echo dual-flip-angle spoiled gradient-recalled MR imaging technique for quantification–a feasibility study. Radiology 2011;259(2):487–94. [PubMed: 21324839]
78. Alizai H, Nardo L, Karampinos DC, et al. Comparison of clinical semi-quantitative assessment of muscle fat infiltration with quantitative assessment using chemical shift-based water/fat separation in MR studies of the calf of post-menopausal women. Eur Radiol 2012;22(7):1592–600. [PubMed: 22411305]
79. Karampinos DC, Baum T, Nardo L, et al. Characterization of the regional distribution of skeletal muscle adipose tissue in type 2 diabetes using chemical shift-based water/fat separation. J Magn Reson Imaging 2012;35(4):899–907. [PubMed: 22127958]
80. Kumar D, Karampinos DC, MacLeod TD, et al. Quadriceps intramuscular fat fraction rather than muscle size is associated with knee osteoarthritis. Osteoarthritis Cartilage 2014;22(2): 226–34. [PubMed: 24361743]
81. Nardo L, Karampinos DC, Lansdown DA, et al. Quantitative assessment of fat infiltration in the rotator cuff muscles using water-fat MRI. J Magn Reson Imaging 2014;39(5):1178–85. [PubMed: 24115490]
82. Stephenson MC, Gunner F, Napolitano A, et al. Applications of multi-nuclear magnetic resonance spectroscopy at 7T. World J Radiol 2011;3(4): 105–13. [PubMed: 21532871]
83. Boesch C Musculoskeletal spectroscopy. J Magn Reson Imaging 2007;25(2):321–38. [PubMed: 17260389]
84. Wang L, Salibi N, Wu Y, et al. Relaxation times of skeletal muscle metabolites at 7T. J Magn Reson Imaging 2009;29(6):1457–64. [PubMed: 19472422]
85. Bogner W, Chmelik M, Schmid AI, et al. Assessment of (31)P relaxation times in the human calf muscle: a comparison between 3 T and 7 T in vivo. Magn Reson Med 2009;62(3):574–82. [PubMed: 19526487]
86. Parasoglou P, Xia D, Chang G, et al. Dynamic three-dimensional imaging of phosphocreatine recovery kinetics in the human lower leg muscles at 3T and 7T: a preliminary study. NMR Biomed 2013;26(3):348–56. [PubMed: 23065754]
87. Minotti JR, Johnson EC, Hudson TL, et al. Training-induced skeletal muscle adaptations are independent of systemic adaptations. J Appl Physiol (1985) 1990;68(1):289–94. [PubMed: 2312472]
88. van Oorschot JW, Schmitz JP, Webb A, et al. 31P MR spectroscopy and computational modeling identify a direct relation between Pi content of an alkaline compartment in resting muscle and phosphocreatine resynthesis kinetics in active muscle in humans. PLoS One 2013;8(9):e76628. [PubMed: 24098796]
89. Schunk K, Romaneehsen B, Rieker O, et al. Dynamic phosphorus-31 magnetic resonance spectroscopy in arterial occlusive disease: effects of vascular therapy on spectroscopic results. Invest Radiol 1998;33(6):329–35. [PubMed: 9647444]
90. Scheuermann-Freestone M, Madsen PL, Manners D, et al. Abnormal cardiac and skeletal muscle energy metabolism in patients with type 2 diabetes. Circulation 2003;107(24):3040–6. [PubMed: 12810608]
91. Towse TF, Childs BT, Sabin SA, et al. Comparison of muscle BOLD responses to arterial occlusion at 3 and 7 Tesla. Magn Reson Med 2016;75(3): 1333–40. [PubMed: 25884888]

Author Manuscript Author Manuscript Author Manuscript Author Manuscript

92. Kim HK, Laor T, Horn PS, et al. T2 mapping in Duchenne muscular dystrophy: distribution of disease activity and correlation with clinical assessments. Radiology 2010;255(3):899–908. [PubMed: 20501727]

93. Carlier PG, Azzabou N, de Sousa PL, et al. Skeletal muscle quantitative nuclear magnetic resonance imaging follow-up of adult Pompe patients. J Inherit Metab Dis 2015;38(3):565–72. [PubMed: 25749708]

94. Arpan I, Willcocks RJ, Forbes SC, et al. Examination of effects of corticosteroids on skeletal muscles of boys with DMD using MRI and MRS. Neurology 2014;83(11):974–80. [PubMed: 25098537]

95. Chang G, Wang L, Schweitzer ME, et al. 3D 23Na MRI of human skeletal muscle at 7 Tesla: initial experience. Eur Radiol 2010;20(8):2039–46. [PubMed: 20309556]

96. Weber MA, Nagel AM, Jurkat-Rott K, et al. Sodium (23Na) MRI detects elevated muscular sodium concentration in Duchenne muscular dystrophy. Neurology 2011;77(23):2017–24. [PubMed: 22116947]

97. Weber MA, Nielles-Vallespin S, Huttner HB, et al. Evaluation of patients with paramyotonia at 23Na MR imaging during cold-induced weakness. Radiology 2006;240(2):489–500. [PubMed: 16775221]

98. Johnell O, Kanis JA. An estimate of the worldwide prevalence and disability associated with osteoporotic fractures. Osteoporos Int 2006;17(12): 1726–33. [PubMed: 16983459]

99. Link TM. Osteoporosis imaging: state of the art and advanced imaging. Radiology 2012;263(1):3–17. [PubMed: 22438439]

100. Sell CA, Masi JN, Burghardt A, et al. Quantification of trabecular bone structure using magnetic resonance imaging at 3 tesla—calibration studies using microcomputed tomography as a standard of reference. Calcif Tissue Int 2005;76(5):355–64. [PubMed: 15868282]

101. Driban JB, Barbe MF, Amin M, et al. Validation of quantitative magnetic resonance imaging-based apparent bone volume fraction in peri-articular tibial bone of cadaveric knees. BMC Musculoskelet Disord 2014;15:143. [PubMed: 24779374]

102. Chang G, Wang L, Liang G, et al. Reproducibility of subregional trabecular bone micro-architectural measures derived from 7-Tesla magnetic resonance images. MAGMA 2011;24(3): 121–5. [PubMed: 21221706]

103. Chang G, Deniz CM, Honig S, et al. MRI of the hip at 7T: feasibility of bone microarchitecture, high-resolution cartilage, and clinical imaging. J Magn Reson Imaging 2014;39(6):1384–93. [PubMed: 24115554]

104. Chang G, Honig S, Liu Y, et al. 7 Tesla MRI of bone microarchitecture discriminates between women without and with fragility fractures who do not differ by bone mineral density. J Bone Miner Metab 2015; 33(3):285–93. [PubMed: 24752823]

105. Chang G, Boone S, Martel D, et al. MRI assessment of bone structure and microarchitecture. J Magn Reson Imaging 2017;46(2):323–37. [PubMed: 28165650]

106. Chang G, Pakin SK, Schweitzer ME, et al. Adaptations in trabecular bone microarchitecture in Olympic athletes determined by 7T MRI. J Magn Reson Imaging 2008;27(5):1089–95. [PubMed: 18425824]

107. Chang G, Rajapakse CS, Babb JS, et al. In vivo estimation of bone stiffness at the distal femur and proximal tibia using ultra-high-field 7-Tesla magnetic resonance imaging and micro-finite element analysis. J Bone Miner Metab 2012; 30(2):243–51. [PubMed: 22124539]

108. Chang G, Rajapakse CS, Diamond M, et al. Micro-finite element analysis applied to high-resolution MRI reveals improved bone mechanical competence in the distal femur of female pre-professional dancers. Osteoporos Int 2013;24(4): 1407–17. [PubMed: 22893356]

109. Chang G, Wang L, Liang G, et al. Quantitative assessment of trabecular bone micro-architecture of the wrist via 7 Tesla MRI: preliminary results. MAGMA 2011;24(4):191–9. [PubMed: 21544680]

110. Techawiboonwong A, Song HK, Wehrli FW. In vivo MRI of submillisecond T2 species with two-dimensional and three-dimensional radial sequences and applications to the measurement of cortical bone water. NMR Biomed 2008;21(1): 59–70. [PubMed: 17506113]

Author Manuscript Author Manuscript Author Manuscript Author Manuscript

111. Du J, Hamilton G, Takahashi A, et al. Ultrashort echo time spectroscopic imaging (UTESI) of cortical bone. Magn Reson Med 2007;58(5): 1001–9. [PubMed: 17969110]

Author Manuscript Author Manuscript Author Manuscript Author Manuscript

KEY POINTS

- The signal-to-noise ratio gain of 7T MR imaging benefits both clinical and research musculoskeletal imaging.
- RF and B_0 inhomogeneity and coil design are the major challenges of MR imaging at 7T.
- Future musculoskeletal imaging protocols will likely be a hybrid of morphologic, compositional, and functional MR imaging sequences.

Author Manuscript Author Manuscript Author Manuscript Author Manuscript

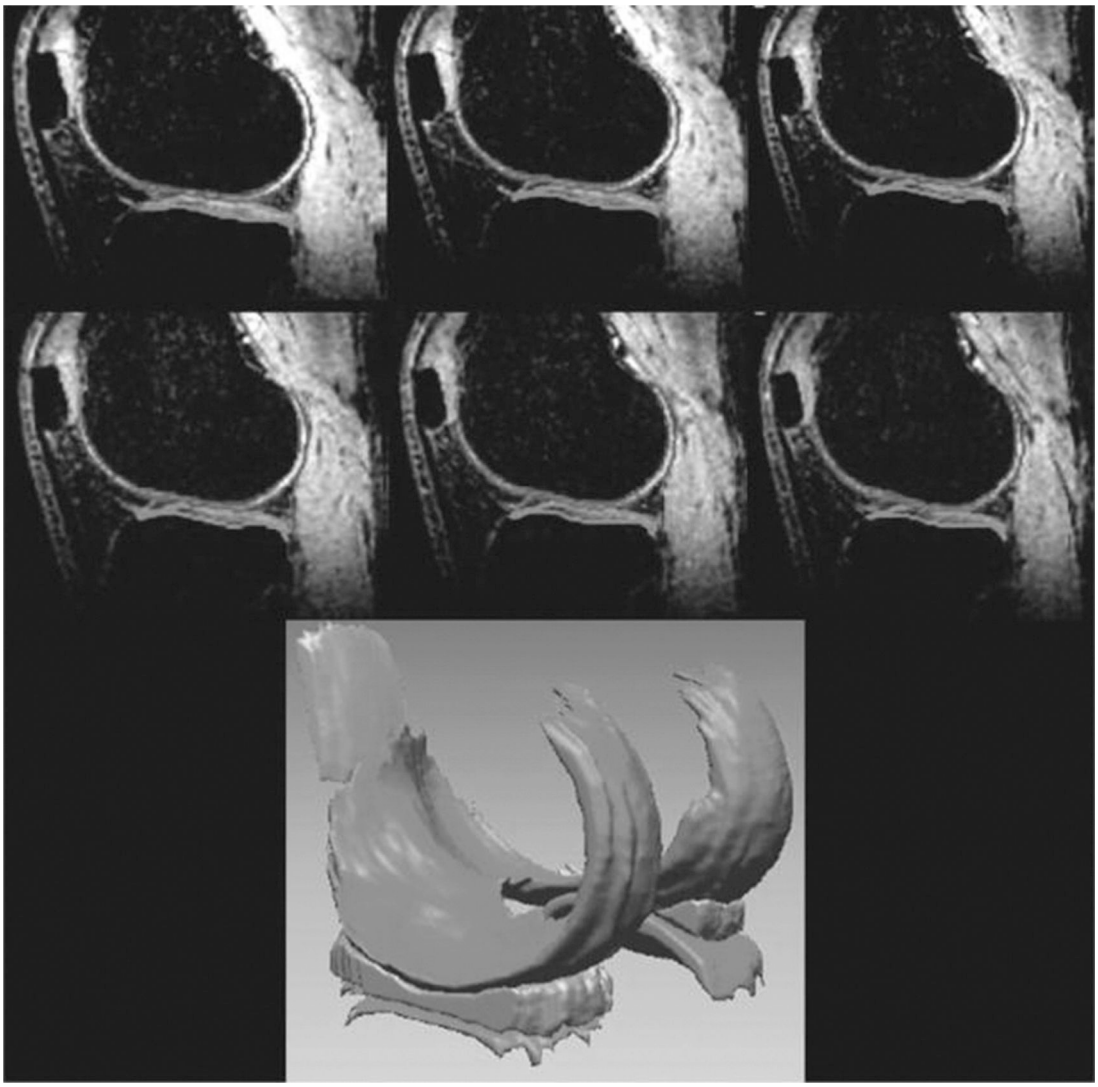

Fig. 1.

Representative high-resolution (3D fast low-angle shot) sagittal knee images with fat suppression were acquired on a healthy volunteer at 7T for better visualization of cartilage and surrounding structures. Three-dimensional cartilage and menisci volume were reconstructed from corresponding segmented regions; 160 slices were acquired in approximately 13 minutes with 500 μm × 500 μm × 500 μm isotropic resolution. (*From* Regatte RR, Schweitzer ME. Novel contrast mechanisms at 3 T and 7 T. Semin Musculoskelet Radiol 2008;12(3):266–80; with permission.)

Author Manuscript Author Manuscript Author Manuscript Author Manuscript

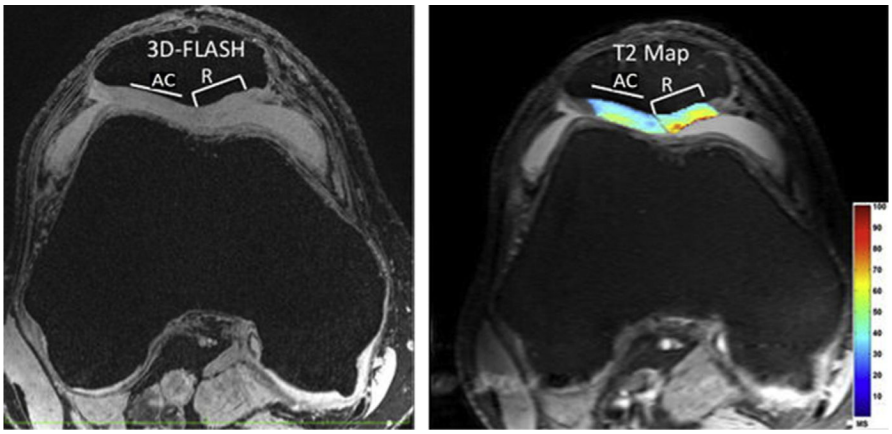

Fig. 2.

Juvenile cartilage cell implantation. High-resolution 7T 3D-FLASH image (*left panel*, repetition time/echo time [TR/TE] = 20 ms/5.1 ms, 0.234 mm × 0.234 mm × 1 mm) and T2 map (*right panel*, TR/TE = 3000 ms/15, 30, 45, 60, 75, 90 ms, 0.586 mm × 0.586 mm × 2 mm) demonstrate close to normal thickness, but higher T2 values in the repair (R) tissue compared with adjacent cartilage (AC). (*From* Chang G, Xia D, Sherman O, et al. High resolution morphologic imaging and T2 mapping of cartilage at 7 T: comparison of cartilage repair patients and healthy controls. MAGMA 2013;26(6):539–48; with permission.)

Author Manuscript Author Manuscript Author Manuscript Author Manuscript

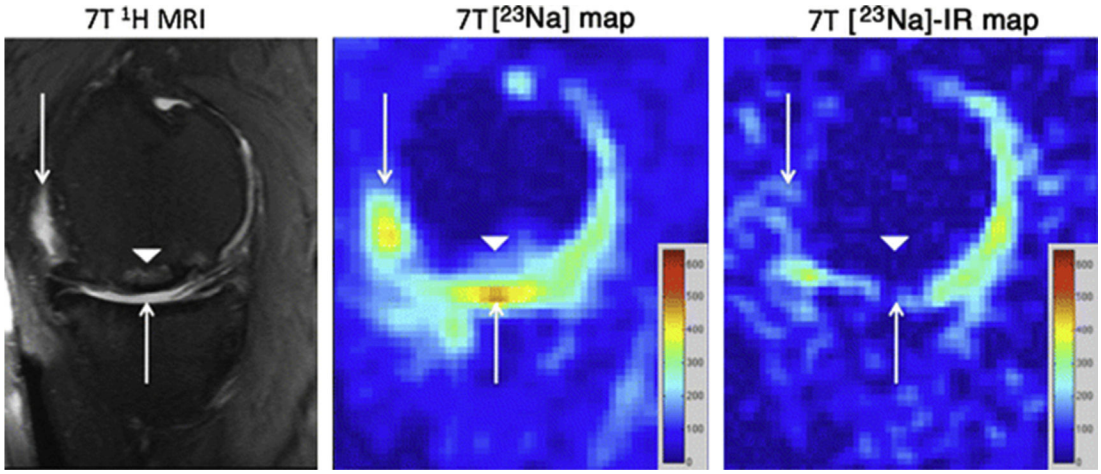

Fig. 3.

Sagittal T2-weighted 7T MR image (*left panel*) of the right knee demonstrating an osteochondral allograft (*arrowhead*) at the weight-bearing aspect of the medial femoral condyle. There is synovial fluid at the articular surface (*arrows*). On the conventional ^{23}Na concentration map (*middle panel*), hyperintense signal is seen from synovial fluid at the articular surface (*arrows*) and to a lesser extent in a subchondral location at the repair site (*arrowhead*). On the sodium concentration map generated from ^{23}Na-IR MR imaging (right panel), there is suppression of signal from free sodium within synovial fluid (*arrows*) and also in the subchondral location (arrowhead). The sodium images represent concentration maps, with colored bars indicating range of [Na^+] in mM (*red* = 600 mM, *blue* = 0 mM). The larger apparent joint space size on sodium maps compared with proton images is likely due to partial volume averaging from the lower resolution of the sodium maps (2 mm × 2 mm × 2 mm vs 0.546 mm × 0.546 mm × 2 mm). (*Reprinted from* Chang G, Madelin G, Sherman OH, et al. Improved assessment of cartilage repair tissue using fluid-suppressed ^{23}Na inversion recovery MR imaging at 7 T: preliminary results. Eur Radiol 2012;22:1341–9; with permission.)

Author Manuscript Author Manuscript Author Manuscript Author Manuscript

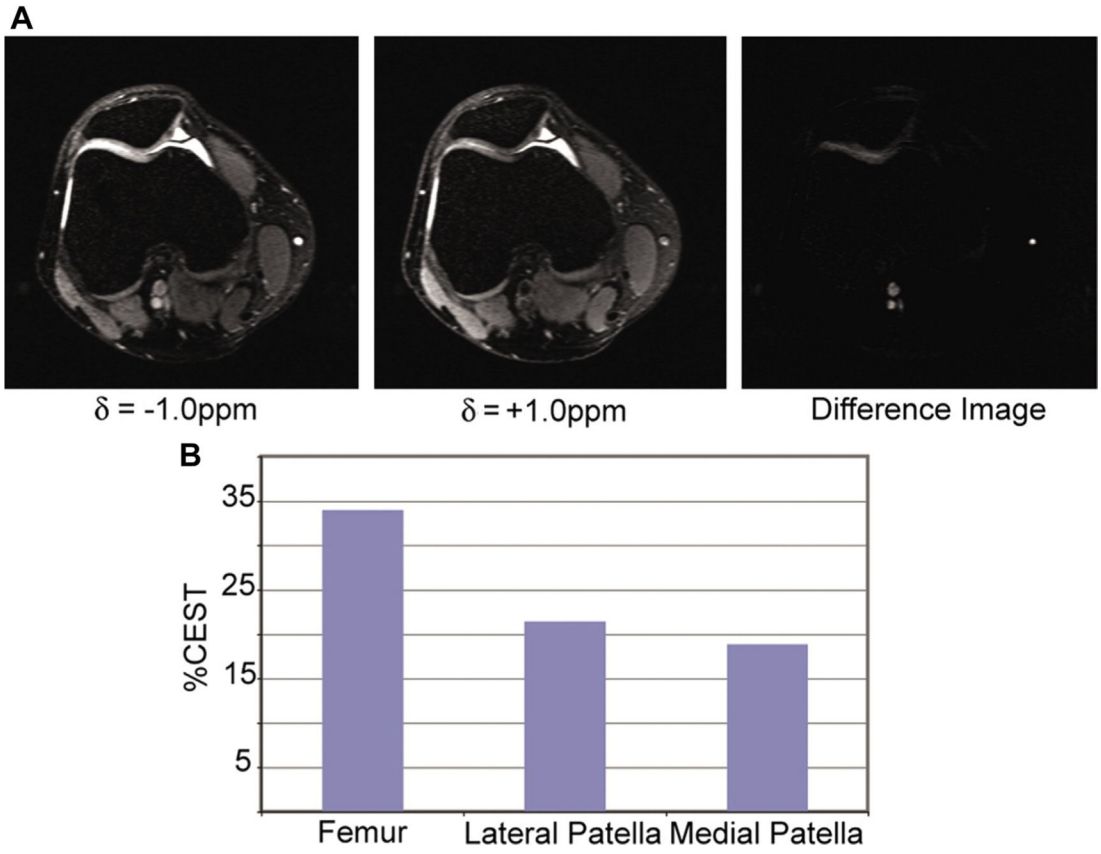

Fig. 4.

Images of a human patella in vivo with irradiation at δ = −1.0 ppm, δ = +1.0 ppm, and the difference image (*A*) along with the extracted CEST contrast from the femur and the lateral and medial sides of the patella (*B*). The total duration of the presaturation pulse sequence was 320 ms at an average rf power of 42 Hz. (*From* Ling W, Regatte RR, Navon G, et al. Assessment of glycosaminoglycan concentration in vivo by chemical exchange-dependent saturation transfer (gagCEST). Proc Natl Acad Sci U S A 2008;105(7):2266–70; © 2008 National Academy of Sciences, U.S.A. with permission.)

Author Manuscript Author Manuscript Author Manuscript Author Manuscript

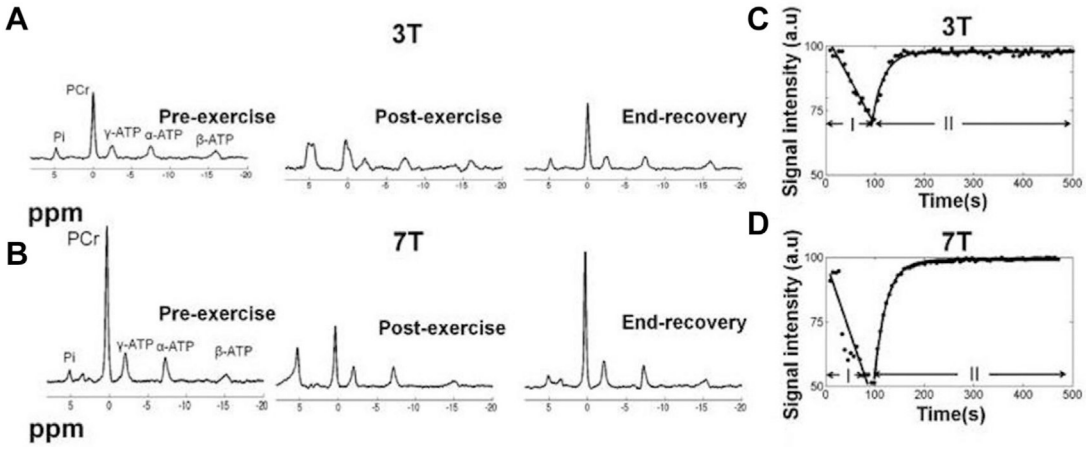

Fig. 5.

MR spectra of the same volunteer before and after exercise, and at the end of the recovery period (*A*) at 3T and (*B*) at 7T. We have normalized the amplitude of all postexercise spectra to the preexercise ones. We observed an almost threefold increase of SNR at 7T relative to 3T. Evolution of the phosphocreatine (PCr) MRS signal intensity during the execution of the exercise (I) and the recovery period (II) from the same volunteer. PCr depletion rates were estimated by fitting a linear function to phase I, whereas the PCr recovery kinetics were characterized by fitting a mono-exponential growth function to phase II of the exercise. (*C*) At 3T, the PCr depletion rate is 0.35 s^{-1} (estimated from the slope of the fitted line, $r = 0.997$) and the recovery rate constant is 22.4 s ($r = 0.981$). (*D*) At 7T, the PCr depletion rate is 0.49 s^{-1} ($r = 0.945$) and the recovery rate constant is 23.89 s ($r = 0.998$). (*From* Parasoglou P, Xia D, Chang G, et al. Dynamic three-dimensional imaging of phosphocreatine recovery kinetics in the human lower leg muscles at 3T and 7T: a preliminary study. NMR Biomed 2013;26(3):348–56; with permission.)

Author Manuscript Author Manuscript Author Manuscript Author Manuscript

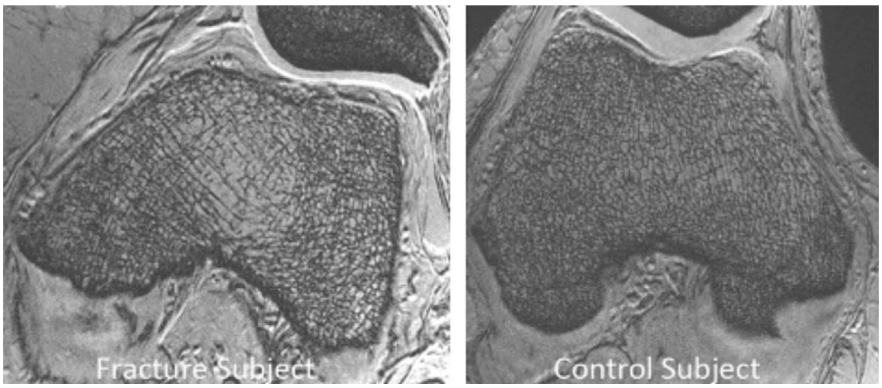

Fig. 6.

MR imaging at 7T reveals deterioration in distal femur trabecular bone microarchitecture in a fragility fracture subject (*left*) compared with a control subject (*right*). The fracture subject demonstrates fewer trabeculae, which are disconnected, and more widely spaced apart. (*From* Chang G, Boone S, Martel D, et al. MR imaging assessment of bone structure and microarchitecture. J Magn Reson Imaging 2017;46(2):323–37; with permission.)

Author Manuscript Author Manuscript Author Manuscript Author Manuscript

Table 1

A summary of potential advantages and disadvantages of high and ultrahigh field systems in musculoskeletal imaging

Characteristic	Trend	Positive	Negative
SNR	↑	Higher resolution, shorter scan time, X-nuclei	NA
SAR	↑	NA	Fewer slices, smaller flip angles
Physiologic side effects (7T)	↑	NA	Dizziness, nausea, metallic taste
Relaxation times	T_1↑		Scan time increase, DWI/DTI
	T_2↓		
	T_2*↓	Facilitates BOLD, SWI at 7T	
RF homogeneity	↓	Parallel reception, parallel transmission	Poor inversion, poor contrast
Susceptibility effects	↑	T_2*	Geometric distortions Metal artifact
Chemical shift	↑	Fat saturation, spectral resolution	Fat/water Misregistration

Abbreviations: BOLD, Blood Oxygen Level Dependent contrast; DTI, diffusion tensor imaging; DWI, diffusion-weighted imaging; NA, not applicable; SAR, specific absorption rate; SNR, signal-to-noise ratio; SWI, Susceptibility weighted imaging; ↑, Increase; ↓, Decrease.

Adapted from Moser E, Stahlberg F, Ladd ME, et al. 7-T MR—from research to clinical applications? NMR Biomed 2012;25(5):695–716; with permission.